



Recent variability and trends and projected changes in precipitation in the southeastern United States: a focus on the Apalachicola-Chattahoochee-Flint River Basin

Jeremy E. Diem¹ · Prince Osei Bonsu¹

Received: 12 September 2023 / Accepted: 18 December 2023

© The Author(s), under exclusive licence to Springer-Verlag GmbH Austria, part of Springer Nature 2023

Abstract

Changes in precipitation impact water availability in river basins; therefore, it is important to perform detailed analyses of precipitation variables within regions to better understand drivers of precipitation variability. This study, which focuses on the Apalachicola-Chattahoochee-Flint River Basin in the southeastern United States, provides an analysis of precipitation variability during 1980–2021 and connects that information to circulation variables while also exploring the alignment between recent and projected precipitation changes. Data include daily precipitation totals from 33 stations, monthly values for circulation indices, and downscaled precipitation projections from climate models. Results show the pressure gradient across the southwestern North Atlantic Ocean and southeastern United States—which is a function of the strength and position of the Bermuda High—is strongly correlated with the precipitation variables and might be an important control of precipitation variability in the basin. In contrast, most teleconnection indices are relatively weakly correlated with precipitation. The basin has generally been getting wetter, with summer having the largest increases in precipitation totals and precipitation days and thus large decreases in maximum consecutive dry days. Increases in heavy-precipitation variables are relatively small, with the largest increases in the northern portion of the basin. Precipitation is projected to increase in the next several decades compared to recent decades, with heavy precipitation expected to have the largest increase. Since the Bermuda High is likely the dominant driver of precipitation in the basin, more information is needed about specific changes to the Bermuda High in upcoming decades to better determine how precipitation might change.

1 Introduction

Recent global warming has impacted precipitation. The current period of global warming dates to the 1970s, after significant reductions in anthropogenic aerosols halted a decades-long hiatus in warming (Jiménez-de-la-Cuesta and Mauritsen 2019). Global surface temperatures increased ~1.2 °C during 1900–2022, with ~0.9 °C of that warming occurring since 1979 (GISTEMP Team 2023). There also has been a concomitant increase in atmospheric water vapor since the 1970s (Allan et al. 2022), resulting from increased sea-surface temperatures (Trenberth 2011). At the global scale, both precipitation totals and heavy-precipitation events should theoretically increase with increased

temperatures (O’Gorman and Schneider 2009; Wetherald 2009). Warming also causes shifts in large-scale circulation, with the primary change being the expansion of the Hadley Circulation (Davis and Rosenlof 2012). The main observed changes in precipitation since the 1970/1980s include the following: an increase in precipitation difference between the wet tropics and dry subtropics; an increase in northern high-latitude annual precipitation over land; and an increase in daily mean precipitation intensities in a majority of land regions (Douville et al. 2021).

One region in the middle latitudes—which has had far from uniform changes in precipitation—that has been sensitive to precipitation variability is the southeastern United States (SEUS). The humid-subtropical climate type prevails across the SEUS (Beck et al. 2018), and this climate is characterized by hot, humid summers and small seasonal differences in precipitation (Trewartha and Horn 1980). Therefore, much of the SEUS has a soil-water surplus during winter and a soil-water deficit during summer (Abatzoglou et al. 2018). Annual precipitation totals range from ~1000

✉ Jeremy E. Diem
jdiem@gsu.edu

¹ Department of Geosciences, Georgia State University, Atlanta, GA 30302, USA

mm to >2200 mm (Kunkel et al. 2013). Severe droughts of short duration do occasionally occur in the SEUS (Seager et al. 2009), and the consequences can be devastating; for example, the 2016 drought, which peaked in October and November, caused millions of dollars of crop losses and widespread wildfires (Williams et al. 2017). In addition, long-term water supply reliability and vulnerability for large metropolitan areas are more sensitive to precipitation totals than to municipal and industrial demand and ambient temperatures (Schlef et al. 2018).

Prior research shows varying teleconnections between precipitation in the SEUS with conditions in the Atlantic and Pacific Oceans. The Atlantic Meridional Oscillation (AMO), which is a shift in sea-surface temperatures (SSTs) in the North Atlantic Ocean, is negatively correlated with precipitation annually and during all seasons (Nigam et al. 2011; Maleski and Martinez 2018). The North Atlantic Oscillation (NAO), which is a shift in standardized sea-level pressure difference between the subtropical and northern portions of the Atlantic Ocean, is positively correlated with winter precipitation in the interior portion and has weak correlations for the SEUS as a whole for the other seasons (Henderson and Vega 1996). The El Niño–Southern Oscillation (ENSO), which is the shift in SSTs across the tropical Pacific Ocean, has its warm phase associated with precipitation totals annually (Maleski and Martinez 2018), precipitation totals in winter only (Henderson and Vega 1996), precipitation totals in winter and autumn (Wang and Asefa 2018), and heavy precipitation in winter (Skeeter et al. 2019). The Pacific–North American teleconnection (PNA) pattern, which affects the strength and location of the jet stream entering North America, is negatively correlated with winter precipitation in the interior portion of the SEUS (Henderson and Vega 1996; Burt et al. 2018) but is positively correlated with precipitation in Florida (Henderson and Vega 1996). Correlations for spring and summer are positive throughout the SEUS (Henderson and Vega 1996).

Prior research also shows that precipitation in the SEUS is connected strongly to the strength and position of the Bermuda High (i.e., North Atlantic Subtropical High), which is located east of the region. Four indices, the Bermuda High Index (BHI), the Western Bermuda High Index (WBHI), the longitude of the western ridge of the Bermuda High, and the latitude of the western ridge of the Bermuda High have been connected to precipitation in the SEUS. The BHI is an index of the difference between normalized sea-level pressure over Bermuda and New Orleans, Louisiana (Stahle and Cleveland 1992). The WBHI is an index of the difference between normalized lower-troposphere pressure over the southwestern North Atlantic Ocean and Louisiana (Diem 2013a). The BHI and WBHI show the pressure gradient across the southwestern North Atlantic Ocean and the southeastern United States; thus, positive values of the indices indicate more moisture

advection into and less atmospheric stability over the SEUS (Henderson and Vega 1996; Diem 2013b). The longitude and latitude of the western ridge, which is the westernmost part of the Bermuda High, are summer-specific (Li et al. 2011). Both the BHI and WBHI are strongly correlated with precipitation, irrespective of season (Henderson and Vega 1996; Burt et al. 2018). Correlations involving the western-ridge location are limited: Diem (2013a) shows for precipitation in the Atlanta region strong negative correlations and weak positive correlations with the latitude and longitude, respectively, of the western ridge.

In general, previous studies show precipitation in the SEUS to have increased annually and during autumn and to have decreased during spring, while precipitation intensity has increased annually and during summer and autumn. The time periods used in the studies are as follows: 1895–2018 (Bishop et al. 2019), 1900–2018 (Li et al. 2022), 1901–2015 (Easterling et al. 2017), 1910–2001 (Michaels et al. 2004), 1932–2003 (Wang et al. 2021), 1948–2012 (Powell and Keim 2015), 1950–2016 (Skeeter et al. 2019), 1950–2018 (Li et al. 2022), and 1960–2017 (Brown et al. 2019). Michaels et al. (2004) and—for two periods—Li et al. (2022) show increased annual precipitation totals, but Brown et al. (2019) show decreased totals. Li et al. (2022), Skeeter et al. (2019), and Brown et al. (2019) report increased annual precipitation intensity. For winter precipitation totals, Brown et al. (2019) show a decrease. Easterling et al. (2017), Powell and Keim (2015), and Brown et al. (2019) report decreased spring precipitation totals. Powell and Keim (2015) show decreased summer precipitation totals, while Wang et al. (2010) and Wang et al. (2021) show increased summer precipitation intensity. Increased autumn precipitation total is reported by Bishop et al. (2019), Easterling et al. (2017), and Powell and Keim (2015), and increased autumn precipitation intensity is reported in Bishop et al. (2019) and Skeeter et al. (2019).

Recent climate-modeling projections of precipitation generally show increased precipitation totals and precipitation intensity for the SEUS over the next several decades to the end of the century. All the results shown below are derived from the simulations of multiple models within CMIP6, which is the sixth phase of the Coupled Model Intercomparison Project. Based on the SSP5-8.5 emissions scenario (i.e., an additional 8.5 W m^{-2} of forcing by the year 2100), the region is projected to receive significantly more precipitation and have significantly more intense precipitation annually when comparing 2020–2059 with 1980–2019 (Rastogi et al. 2022) and have an increasing trend in annual precipitation, except in Florida, during 2015–2100 (Marvel et al. 2021). Also using the SSP5-8.5 scenario along with the SSP2-4.5 (i.e., additional 4.5 W m^{-2} of forcing) and SSP1-2.6 (i.e., additional 2.6 W m^{-2} of forcing) scenarios, the region is projected to receive significantly increased precipitation annually when comparing

three periods (2021–2040, 2041–2060, and 2080–2099) with 1995–2014, and there is little difference among the three scenarios with respect to precipitation projections (Almazroui et al. 2021). Using the three scenarios, precipitation intensity and number of precipitation days are projected to be larger in 2081–2100 compared to 1995–2014, with much more agreement among models for changes in precipitation intensity than changes in precipitation days (Douville et al. 2021). And based on the SSP2-4.5 scenario using the same time periods as above, annual and seasonal precipitation totals in the region are projected to increase but with low model agreement (Douville et al. 2021).

As can be gleaned from the preceding paragraphs, there has been substantial research on recent and projected precipitation changes in the SEUS, but no single study has provided a detailed analysis of recent precipitation variability and attempted to connect that information to circulation variables while also exploring the alignment between recent and projected precipitation changes. Therefore, the objectives of this study are as follows: (1) to assess recent multi-decadal trends (i.e., trends within the recent global warming period) in multiple precipitation variables at the annual and seasonal scales; (2) to determine the temporal relationships between the precipitation variables and teleconnection and regional-circulation indices; and (3) to examine the congruence between current precipitation changes with precipitation projections.

2 Study region

The Apalachicola-Chattahoochee-Flint (ACF) River Basin is an ideal region for assessing precipitation variability and changes in the SEUS (Fig. 1). The ACF basin, which is located in the center of the SEUS, has a 585 km latitudinal extent, with the far northern region and southern regions having the following major differences: (1) the northern region has more extra-tropical cyclones and associated fronts, especially during the cool season; (2) orographic lifting exists in the northern region; and (3) the southern region has daytime thunderstorm activity in the summer associated with land-ocean thermal contrasts (Kunkel et al. 2013). Precipitation is extremely important in the ACF basin, because water is an increasingly critical resource involving a variety of stakeholders that has led to the longest interstate water conflict—which involves Alabama, Florida, and Georgia—in US history (Wong and Bosman 2014). The two largest users of water, municipal consumption and agriculture, are of roughly equal magnitudes, while the third-largest water user, thermoelectric power, is approximately half those magnitudes (Lawrence 2016). Surface-water withdrawals for municipal water occur primarily in the northern portion of the basin (i.e., the Atlanta metropolitan area) (Feldman 2008). The withdrawals come mostly from Lake Lanier, which is located anomalously far upstream for a large water source for a

metropolitan area (Chattahoochee River Keeper 2023) (Fig. 1). Municipal water demand has increased and is projected to continue increasing: the population of the 11-county Atlanta metropolitan area (see Fig. 1) doubled during 1980–2021 to reach five million persons (U.S. Census Bureau 1996) and is projected to reach 7 million persons in 2050 (Atlanta Regional Commission 2020). The substantial consumptive use by agriculture occurs in the central and southern portions of the basin, which is mostly in Georgia (Wong and Bosman 2014). Much of the withdrawn water is groundwater (Lawrence 2016), and during droughts, there is excessive irrigation using groundwater, thereby depleting aquifers (Mitra et al. 2016). Finally, the basin provides freshwater flow to Apalachicola Bay, an estuary that provides a large share of the nation's seafood and is dependent on consistent flows of the Apalachicola River (Feldman 2008; Schlef et al. 2018). Florida has blamed collapses of oyster harvests in the Apalachicola Bay on Georgia's water consumption in the basin (Schmitz and McCreary 2022).

3 Data and methods

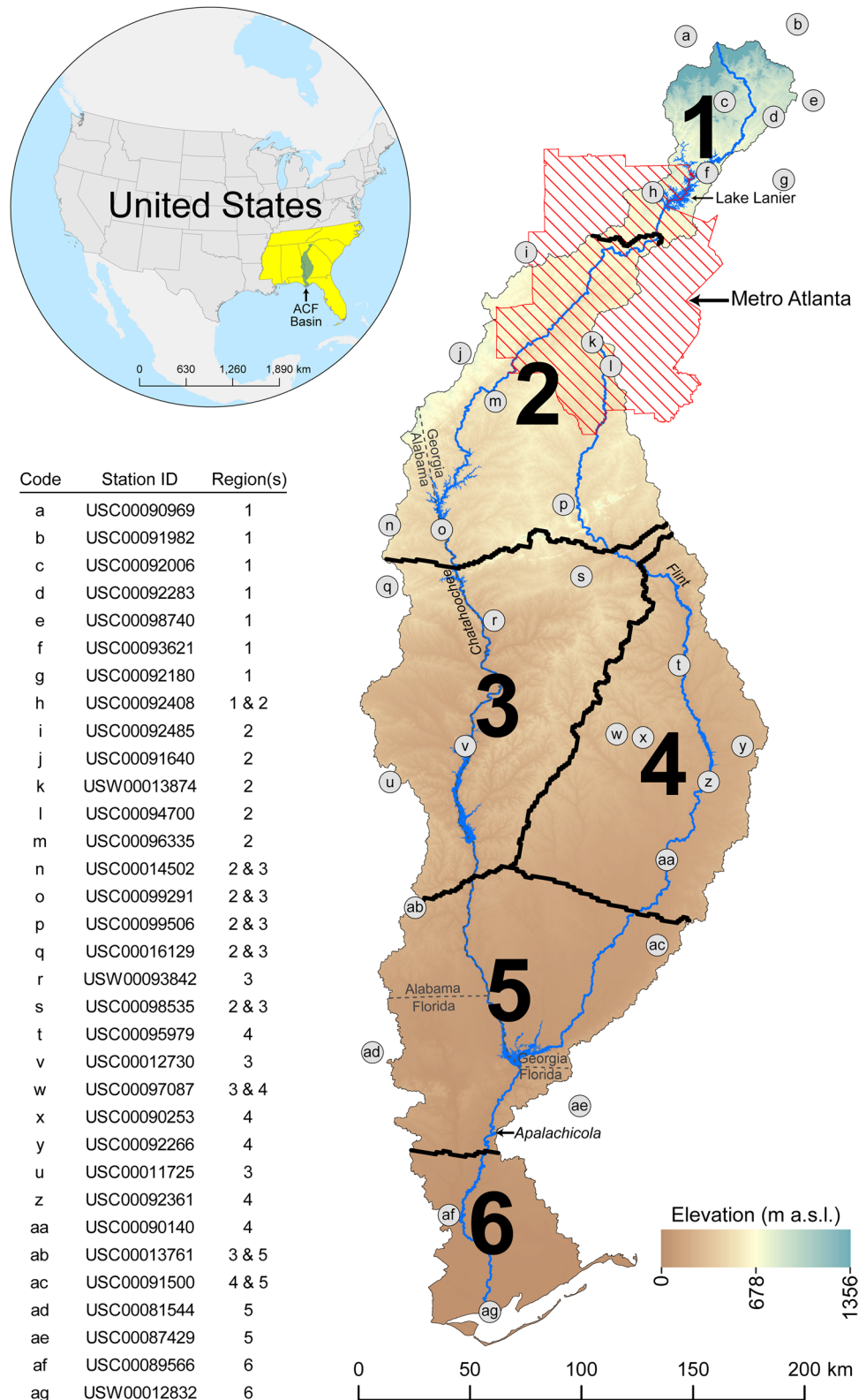
3.1 Precipitation regionalization

The ACF was divided into precipitation regions, and analyses were performed separately for each region. Gridded monthly precipitation totals for 1980–2021 used for the precipitation regionalization were obtained from the DAYMET database of the Oak Ridge National Laboratory (ORNL) (Thornton et al. 2022). DAYMET data were selected because of the high spatial resolution (1 km²) of the grid cells. Principal component analysis (PCA) and *k*-means clustering were the main procedures used for the regionalization; these two procedures are used in other studies (e.g., Marston and Ellis 2020; Jamshidi and Nozar 2022) to delineate precipitation regions. A T-mode input matrix (i.e., rows were grid cells and columns were monthly precipitation totals) was used in the PCA. Scree plots (i.e., plots of explained variance for components), which are standard tools in PCA (Kachigan 1991), were used to determine the optimal number of components to retain. The elbow method (i.e., plots of explained variance as a function of number of clusters) was used with *k*-means clustering of the component scores to determine the optimal number of precipitation regions, and, ultimately, each of the pixels was placed in one precipitation region. The elbow method is used successfully in other studies (e.g., Zhang et al. 2016, Lai et al. 2021).

3.2 Precipitation stations

Data obtained during 1980–2021 at 33 precipitation stations that were part of the Global Historical Climatology Network of the National Oceanic and Atmospheric Administration

Fig. 1 The six precipitation regions and associated stations within the Apalachicola-Chat-tahoochee-Flint (ACF) River Basin. The inset map shows the location of the Apalachicola-Chattahoochee-Flint (ACF) basin within the southeastern United States



(NOAA) and within the ACF and within 20 km of the ACF were used for correlation, trends, and regression analyses (Fig. 1). All stations had at least 80% of daily data during

1980–2021. For the entire 33-station database, only 5.9% of station-days were missing precipitation totals. Stations were either within a region or within 20 km of the region. If

a station had a precipitation observation that occurred in the morning, that precipitation was shifted to the previous day. For each precipitation region, each daily precipitation total was the mean of the stations within the domain (i.e., basin or region) and stations within 20 km of the domain. Using the mean value from multiple stations helped to minimize the impacts of inhomogeneities (Easterling and Peterson 1995). Daily precipitation totals for the basin were weighted means of the regional values (i.e., the weights were the proportional coverages of the regions).

3.3 Precipitation variables

Multiple precipitation variables were calculated at the annual and seasonal scales for the ACF basin and the precipitation regions. The seasons were winter (i.e., December–February), spring (i.e., March–May), summer (i.e., June–August), and autumn (i.e., September–November). The variables were precipitation totals and precipitation days (i.e., days with ≥ 1 mm) along with the following variables recommended by the World Climate Research Programme’s Expert Team on Climate Change Detection and Indices: precipitation intensity, 90th percentile of precipitation totals on precipitation days, heavy-precipitation days, and maximum number of consecutive dry days. Precipitation intensity was the mean precipitation total of precipitation days.

3.4 Correlations between precipitation variables and circulation indices

Temporal correlations between the six precipitation variables—for the entire ACF and the precipitation regions—and multiple circulation indices were calculated at the annual and seasonal scales from 1980 to 2021. All time series were detrended using linear regression, and all subsequent analyses were performed using residuals. Correlations were assessed using Pearson product-moment correlation tests ($\alpha = 0.05$; two tailed). The circulation indices were the AMO index, NAO index, the Niño3.4 index, the PNA index, the BHI, the WBHI, and location of the western ridge of the Bermuda High in summer. AMO, NAO, and PNA indices were obtained from the NOAA’s Climate Prediction Center. The Niño3.4 index—the chosen ENSO index for this study because the Niño3.4 region (5°N – 5°S , 120° – 170°W) is the key region for coupled ocean-atmosphere interactions in ENSO (Trenberth, 1997)—was obtained from NOAA’s Physical Sciences Laboratory. The BHI, WBHI, and location of the western ridge of the Bermuda High were calculated using North America Regional Reanalysis data obtained from NOAA. For the BHI, monthly sea-level pressure values were acquired for grid cells corresponding to 32.5°N and 64°W and 30°N and 90°W . For the WBHI, monthly 850-hPa geopotential

heights were acquired for grid cells corresponding to 30°N and 75°W and 30°N and 92°W . The location of the summer western ridge is the point where the 1560-m line at 850 hPa intersects the ridge line of the Bermuda High (Li et al. 2011).

3.5 Trends in precipitation and circulation variables

Trends in precipitation and circulation variables over 1980–2021 were calculated. The trends, which were assessed using Kendall tau correlation tests ($\alpha = 0.05$; two tailed), were calculated at the annual and seasonal scales. Trends in precipitation variables also were calculated at the basin and regional scales. The Kendall-Theil robust line, the median of the slopes between all combinations of two points in the data (Helsel and Hirsch 2002), was used to estimate changes over the 42-year period.

3.6 Atmospheric circulation and precipitation variability

Multiple-linear regression models were developed to determine the nature of relationships between circulation variables and precipitation at the annual and seasonal scales. PCA was used to screen the circulation variables that were potential predictor variables in the regression models with the precipitation variables as predictands. The screening was performed to ensure that the regression models did not have multicollinearity (Kachigan 1991). The screening was performed at the annual scale and for each of the seasons. For the five separate PCAs, each circulation variable was associated with the component on which it loaded the highest. All circulation variables except western-ridge longitude and latitude were potential predictors in all models. Western-ridge longitude and latitude were only potential predictors in the summer models. Only circulation variables that loaded highly on different components were included as the initial predictors, and a backward-elimination procedure was used to remove variables that were not contributing significantly to the models.

3.7 Precipitation projections

Projected changes in the six precipitation variables under future global warming were examined. Daily, gridded, downscaled precipitation estimates from 1980 to 2059 were obtained from ORNL. The data were downscaled projections based on a six-member General Climate Model (GCM) ensemble—under the SSP5-8.5 emission scenario from CMIP6 (Kao et al. 2022). The spatial resolution of the data was 4 km^2 . For the entire basin and the

precipitation regions at the annual and seasonal scales, 2020–2059 estimates were compared with 1980–2019 estimates. Mann-Whitney U tests ($\alpha = 0.05$; two tailed) were used to identify significant inter-epochal differences.

4 Results

4.1 Characteristics of the precipitation regions

The ACF was divided into six precipitation regions, which had considerable differences in precipitation totals, frequency, intensity, and consecutive dry days for the seasons (Figs. 1 and 2). Annual precipitation totals exceeded 1500 mm in the most northern and mountainous region (i.e., region 1) and the most southern and coastal region (i.e., region 6), while totals in the central portion were approximately 1300 mm. The largest disparity in seasonal precipitation occurred for summer, when region 6 had on average roughly 50% more precipitation than the other regions (Fig. 2a). For winter, spring, and autumn, approximately 35% of days had precipitation for the ACF as a whole (Fig. 2b). For those three seasons combined, region 6 had approximately 20% fewer precipitation days. Precipitation days throughout the basin increased in summer, with all regions having precipitation on at least 50% of days. The PI and P90 values across the regions and seasons were 9.7 mm day^{-1} and 25 mm, respectively (Fig. 2c, d). PI and P90 were approximately 30% and 20% larger, respectively, in winter, spring, and autumn than in summer. Across all seasons, PI and P90 were approximately 25% and 30% larger, respectively, for region 6 than for the other regions. The number of HPDs was relatively small; therefore, it is difficult to summarize inter-seasonal and inter-regional differences in HPDs (Fig. 2e). Seasonal maximum CDDs were largest in autumn and smallest in summer (Fig. 2f). The totals for autumn were typically twice that for summer. Region 6, which had the largest maximum CDDs among the regions for all seasons combined, also had a large number of maximum CDDs in spring.

4.2 Stations per rainfall region

The northern precipitation regions had many more precipitation stations than did the southern regions, with all of the regions having small inter-annual variabilities in station counts (Fig. 3). The mean number of stations for regions 1, 2, 3, 4, 5, and 6 were eight, ten, nine, seven, four, and two, respectively. The coefficients of variation for station counts over the 42-year period ranged from 0.03 for region 6 to 0.09 for regions 3 and 5.

4.3 Correlations between precipitation variables and circulation indices

Most correlations with the AMO tended to be negative, stronger in the southern regions than in the northern regions, and strongest in winter and weakest in spring and summer (Fig. 4). In winter, all precipitation variables were negatively correlated with the AMO, significant correlations existed for all variables, and the southern regions had more significant correlation than did the northern regions. There were no significant correlations in spring and summer. Significant negative correlations reappeared in autumn but did not involve the heavy-precipitation variables.

Correlations with the NAO were generally weak, but there was a large shift from strong negative correlations in spring to strong positive correlations in summer (Fig. 4). There were almost no significant correlations in autumn and winter. There were significant negative correlations in spring, and those correlations involved the heavy-precipitation variables and the inverse of maximum CDD. Summer had significant positive correlations with PT and PD for every region.

Nearly all correlations with Niño3.4 were positive, with the correlations strongest in winter and autumn and in the northern regions (Fig. 4). All variables, except the inverse of maximum CDD, had significant correlations involving at least three regions in winter. Compared to winter, the number of significant correlations was markedly smaller in autumn. In spring and summer, the correlations were weak and there were virtually no significant correlations.

All correlations with the PNA were weak (Fig. 4). The strongest correlations were in winter, and the southern regions tended to have stronger correlations than did the northern regions. The only significant correlations, which were negative, occurred at the annual scale.

Strong correlations with the BHI and WHBI existed annually and during all seasons (Fig. 4). Significant correlations with the BHI were prevalent across the variable/region combinations during winter and autumn. Spring and summer lacked significant correlations with the heavy-precipitation variables and the inverse of maximum CDD, respectively. With respect to the WBHI, there were significant correlations with PT and PD for all season/region combinations. While all seasons had significant correlations with HPD, only summer had all significant correlations. On the other hand, summer had the fewest significant correlations with the inverse of maximum CDD.

Correlations with the position of the western ridge of the Bermuda High—which were only calculated for the summer—showed that the precipitation should change much more with latitudinal position than with longitudinal position (Fig. 4). Correlations with longitude (WR_{long}) were of mixed sign and none of the correlations was significant.

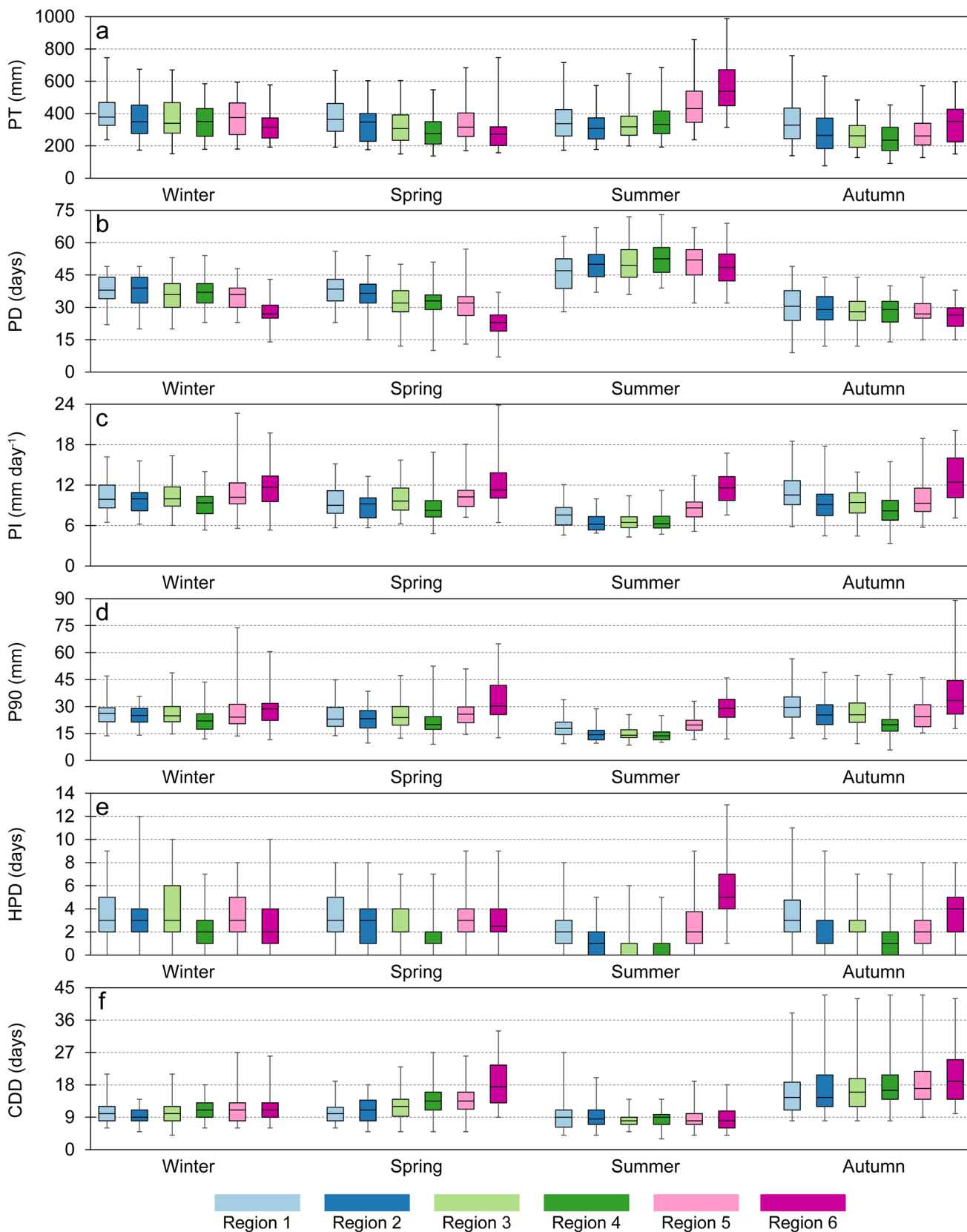


Fig. 2 Box and whisker plots of **a** precipitation totals (PT), **b** precipitation days (PD), **c** precipitation intensity (PI), **d** the 90th percentile of daily precipitation totals (P90), **e** heavy-precipitation days (HPD),

and **f** maximum consecutive dry days (CDD) for the six precipitation regions at the seasonal scale

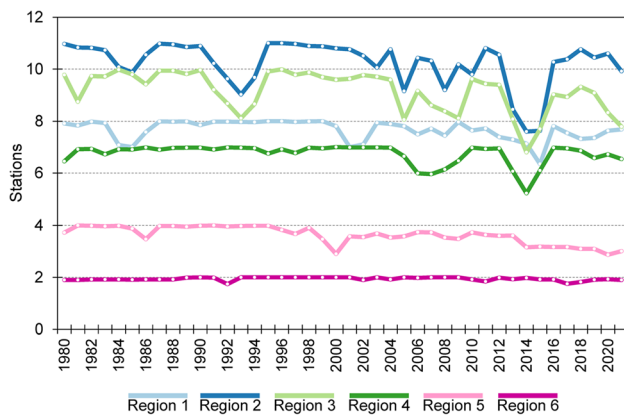


Fig. 3 Changes over time in the number of precipitation stations contributing data to the precipitation regions

Nearly all correlations with latitude (WR_{lat}) were negative and were generally stronger for the northern regions than for the southern regions. Significant correlations were restricted mostly to PT and PI.

4.4 Recent precipitation changes

PT increased for most combinations of spatial domains and temporal units, but only two of the trends were significant (Fig. 5a). The significant trends were a 23% increase for region 5 annually and a 37% increase for region 1 during summer. At the annual scale, all regions except region 6 had increases of at least 10%. PT increased the most in summer and winter, with basin-wide increases of 22% and 17% respectively. The largest increase and decrease for all the region/season combinations were 37% for region 1 during summer and 15% for region 6 during spring, respectively.

PD also increased in general, but the significant increases were mostly restricted to summer (Fig. 5b). All the summer changes were positive, with the summer increase for the entire ACF being 20% and the significant increases occurring for the ACF and regions 2, 3, 4, and 5. There were mostly PD increases annually and during the winter, but only region 3 had significant increases.

Values of the heavy-precipitation variables mostly increased; however, the consistency and magnitude were much weaker than those for PT and PD (Fig. 5c, d, e). Autumn was the only season with PI, P90, and HPD increases for the entire ACF and all regions. Only region 1 had significant increases for PI, P90, and HPD, and the mean increases in those three variables for region 1 were 18%, 28%, and 47%, respectively.

Significant trends in maximum CDD were restricted to spring and summer, and those seasons had opposite changes (Fig. 5f). Maximum CDD increased for all spatial domains in spring, with significant trends for regions 3 and 5. The

mean increase based on all domains was approximately 30%, while regions 3 and 5 had increases of 44% and 35%, respectively. All spatial domains had significant trends in summer, and the mean decrease was approximately 35%.

4.5 Recent trends in circulation indices

Excluding trends in AMO, significant trends in the circulation indices occurred mostly during summer (Fig. 6). AMO increased annually and during all seasons. PNA decreased during spring and increased during summer. BHI increased annually and during summer. WBHI increased during summer. WR_{long} increased (i.e., western ridge moved eastward) during summer, which was the only season when the variable was examined. Niño3.4 and the WR_{lat} did not have any significant trends.

4.6 Circulation contributors to multi-decadal variance in precipitation variables

The amount of variance in precipitation variables explained by circulation variables differed substantially among the temporal units and among the precipitation variables (Fig. 7). The mean coefficients for the annual, winter, and summer models ranged from 0.47 to 0.58, while the mean coefficients for the spring and autumn models ranged from 0.27 to 0.39. In fact, the summer models explained on average over twice as much of the variance compared to the spring models. Across all temporal units, the largest coefficients occurred for PT, PD, and HPD: the mean coefficients for those variables ranged from 0.50 to 0.59. The models had much lower coefficients for PI, P90, and inverse of maximum CDD. The models with the two largest coefficients, which were greater than 0.70, were PT and PD during summer. The models with the two smallest coefficients, which were less than 0.15, were PI and P90 during spring.

All circulation indices except for WR_{long} appeared in at least one model, and either the WBHI or BHI was the most important predictor in nearly all models (Fig. 7). WBHI was the most prevalent predictor: it appeared in 70% of models. Niño3.4 and the BHI occurred in 33% and 30% of models, respectively, and were thus the other more frequent predictors. Niño3.4 appeared mostly in the annual, winter, and autumn models. The WBHI, BHI, and Niño3.4 always had positive coefficients. The WBHI was the most important predictor of precipitation in most annual, spring, summer, and autumn models. AMO, NAO, and PNA indices were relatively weak predictors and all three indices had both positive and negative coefficients. The weakest predictor on average was WR_{lat} .

4.7 Projected changes in precipitation variables

Mean projections from six climate models indicated that the ACF should be wetter during 2020–2059 compared to

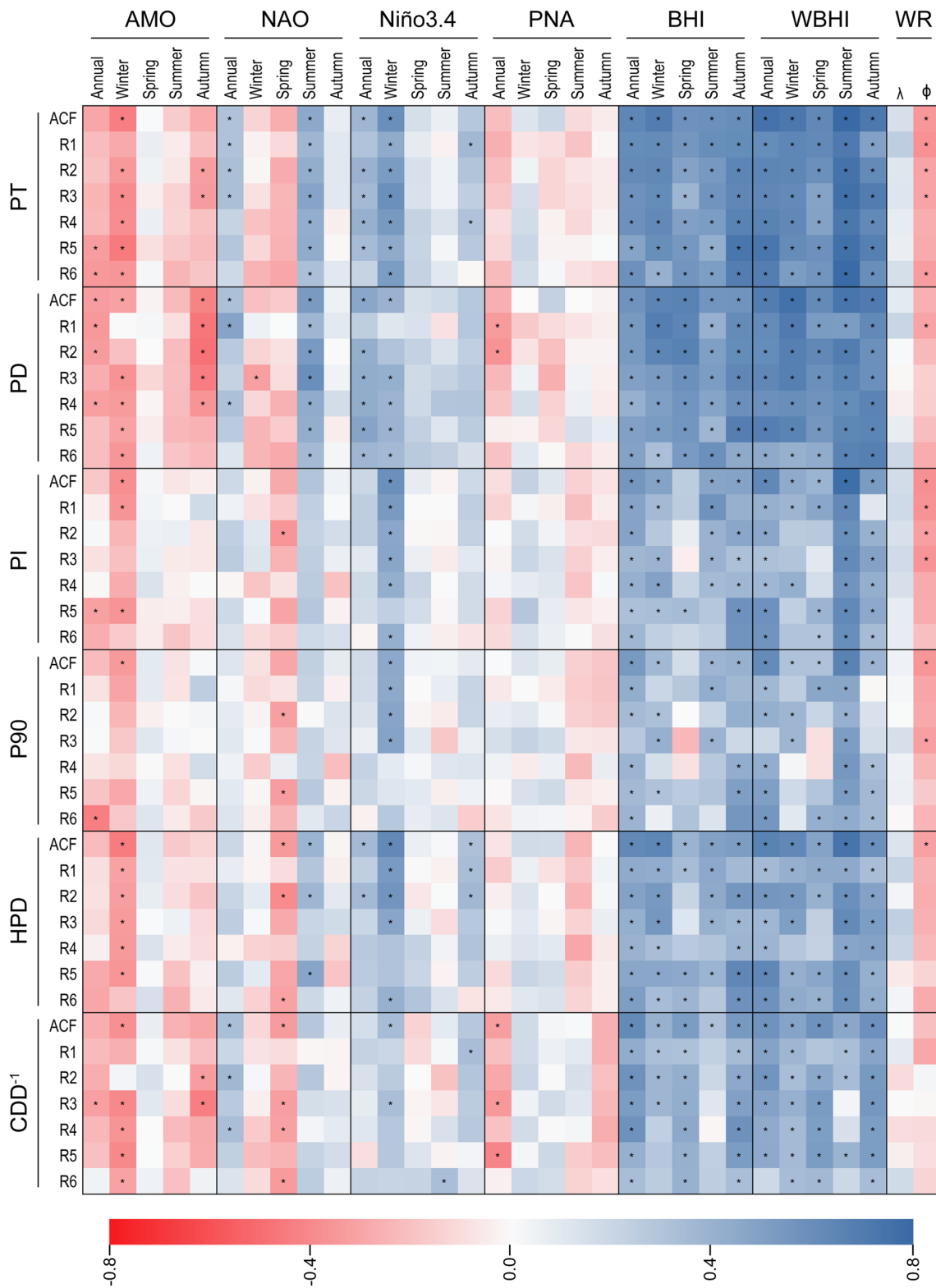


Fig. 4 Annual- and season-specific correlations between the precipitation variables and the Atlantic Multidecadal Oscillation (AMO) index, the North Atlantic Oscillation (NAO) index, the Niño3.4 index, the Pacific North American Index (PNA), the Bermuda High

Index (BHI), the Western Bermuda High Index (WBHI), and the longitude (λ) and latitude (ϕ) of the western ridge of the Bermuda High. Full names of the precipitation variables are provided in the caption for Fig. 2

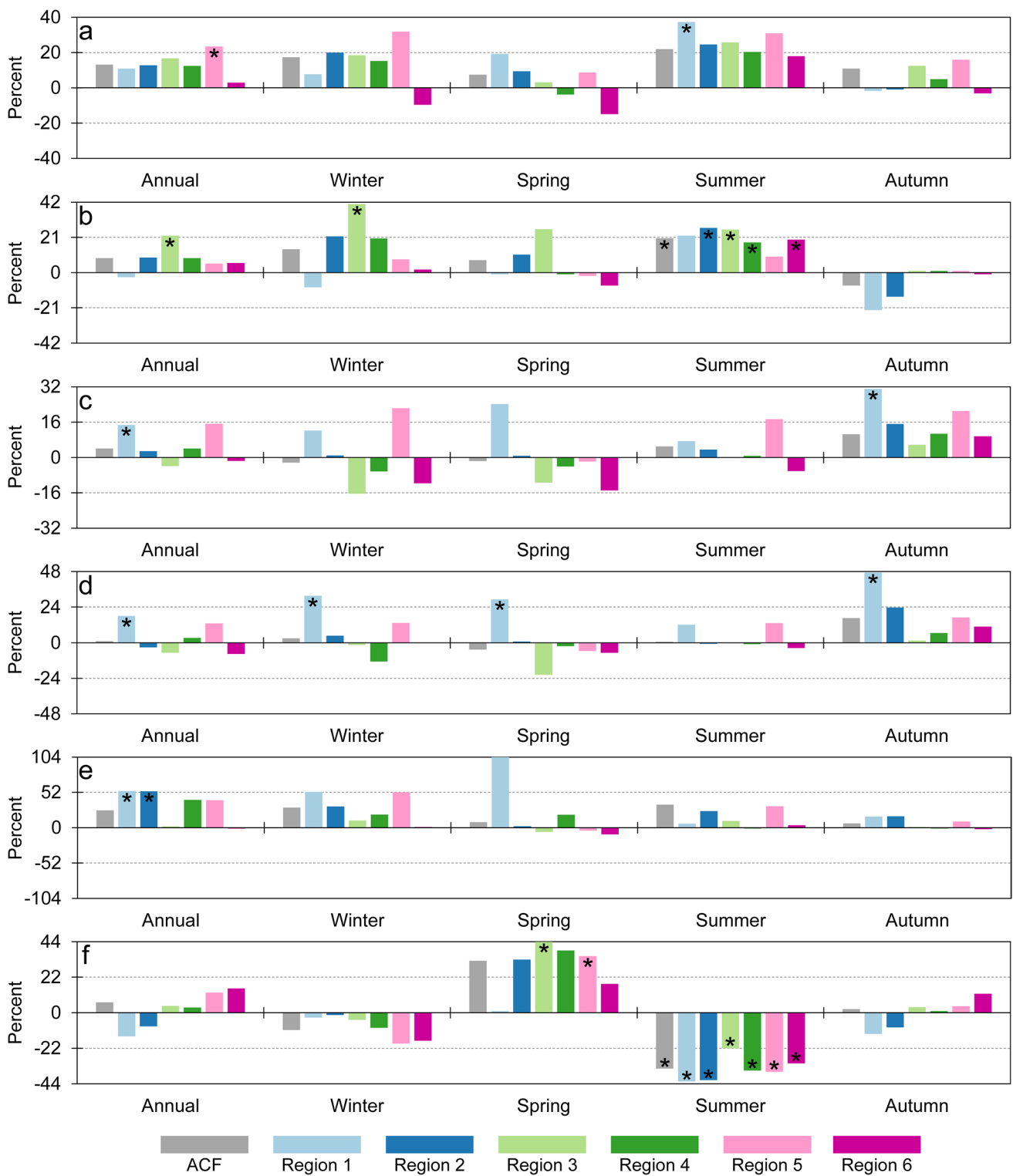


Fig. 5 Annual- and season-specific percent changes for the entire basin and the six precipitation regions during 1980–2021 in **a** precipitation totals, **b** precipitation days, **c** precipitation intensity, **d** the 90th

percentile of daily precipitation totals, **e** heavy-precipitation days, and **f** maximum consecutive dry days. Asterisks denote significant ($\alpha = 0.05$; two-tailed) trends for 1980–2021

Fig. 6 Trends in the circulation indices—as indicated by Kendall’s tau correlation coefficients—over 1980–2021. Asterisks denote significant ($\alpha = 0.05$; two tailed) trends. Full names of the circulation indices are provided in the caption for Fig. 4

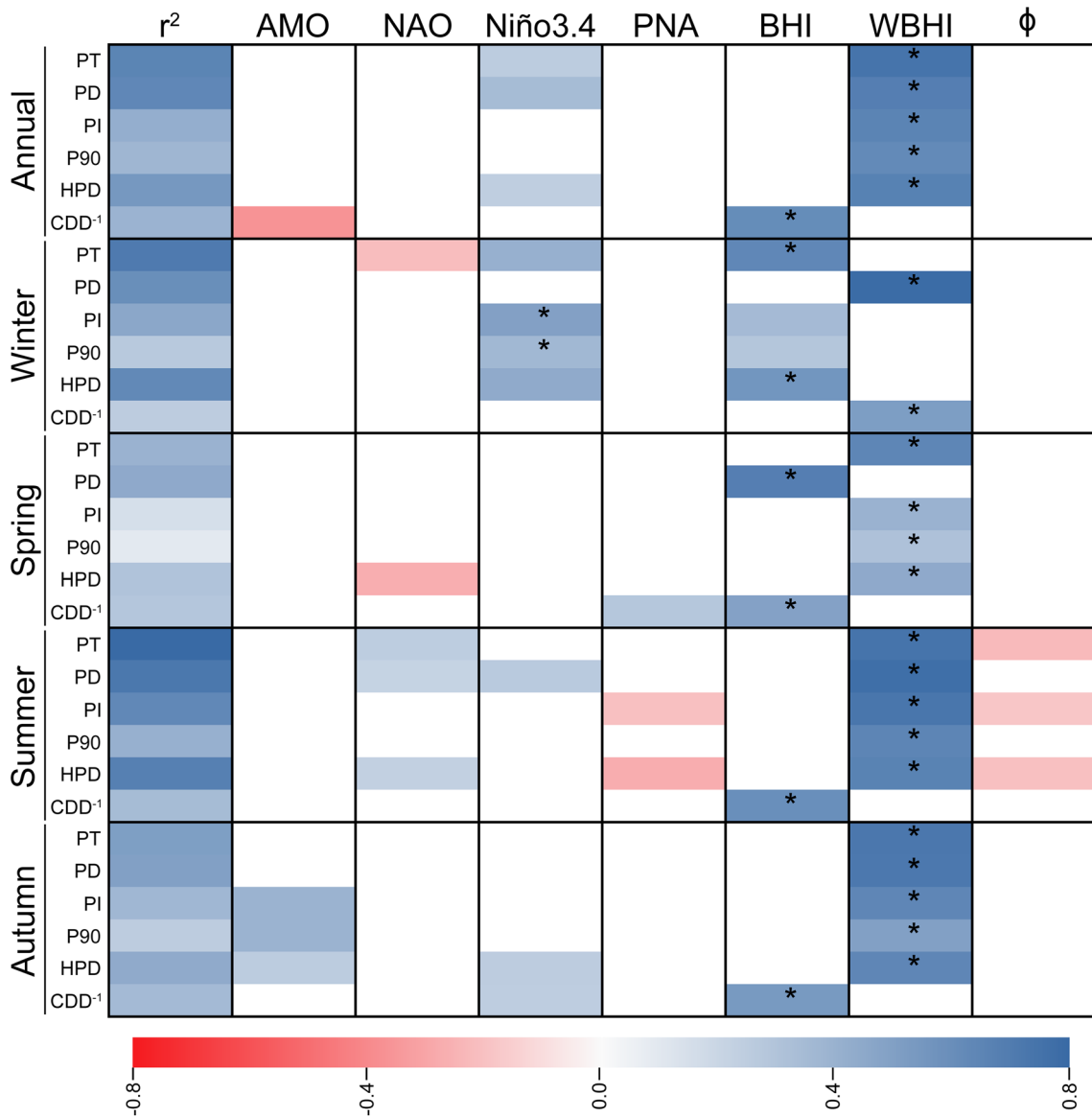
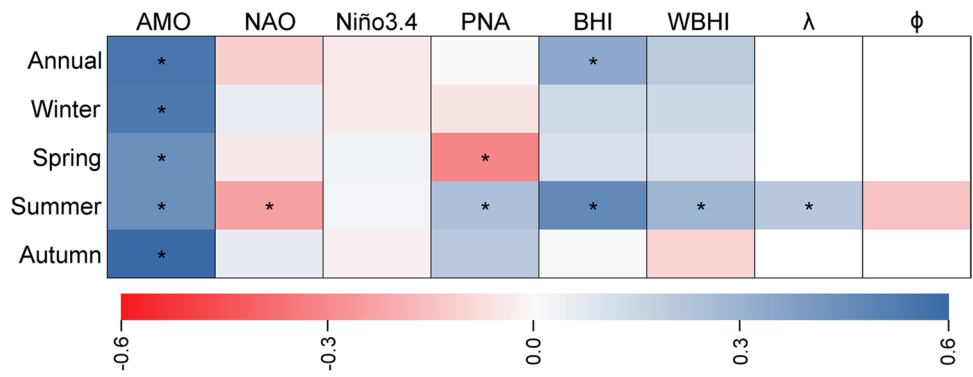


Fig. 7 Coefficients of determination (r^2) and circulation-index standardized slope coefficients for the linear regression models developed for the precipitation variables annually and for each season. An asterisk denotes the variable with the largest standardized slope coefficient

for a model. Full names of the precipitation variables are provided in the caption for Fig. 2. Full names of the circulation indices are provided in the caption for Fig. 4

1980–2019 (Fig. 8). PT and values for the heavy-precipitation variables were projected to increase significantly annually and during all seasons for most regions. On average, PT, PI, P90, and HPD were projected to increase by 7%, 6%, 8%, and 14%, respectively. The largest percentage increases in PT, PI, and P90 were projected to occur in autumn in the southern regions. The largest percentage increase in HPD was projected to occur in summer. PD did not have any significant changes; however, 80% of the changes were positive. Most of the changes for maximum CDD were positive, but only two of the changes were significant.

5 Discussion

5.1 Precipitation variability is driven mostly by characteristics of the Bermuda High, rather than by teleconnection indices

The pressure gradient across the southwestern North Atlantic Ocean and SEUS—which the BHI and WBHI measure—is strongly correlated with the precipitation variables and appears to be an important control of precipitation variability in the ACF. Most correlations between either the BHI or WBHI and the precipitation variables across the temporal units were positive and significant (Fig. 4). Therefore, most correlations with WR_{lat} were negative; the analyses were restricted to summer. Similar findings for the BHI exist for most portions of the SEUS during all seasons (Henderson and Vega 1996), the BHI and WBHI and TP, PD, and HPD during most seasons in a portion of the southern Appalachian Mountains (Burt et al. 2018), and the BHI and WBHI and PT, PD, and HPD in the Atlanta region during summer (Diem 2013a). Significant negative correlations with WR_{lat} also are present in Diem (2013a). Either the WBHI or BHI was the most important predictor in nearly all models (Fig. 7). The WBHI also has been found to be the most important predictor of summer precipitation totals in the Atlanta region (Diem 2013a).

Compared to the BHI and WBHI, teleconnection indices are generally not as strongly correlated with ACF precipitation and—with the exception of Niño3.4—are relatively weak determinants of precipitation variability in the basin. The AMO is negatively correlated with precipitation, which confirms the findings in Nigam et al. (2011) and Maleski and Martinez (2018). The findings in this paper for precipitation correlations with the NAO during summer are similar to those in Burt et al. (2018) in the southern Appalachians: both studies show strong positive correlations. This study also reports strong positive correlations in winter, which also is shown in Henderson and Vega (1996) for the interior portion of the SEUS. The significant positive correlations between Niño3.4 and precipitation annually and during winter—and

to a lesser degree during autumn—align with ENSO correlations in Henderson and Vega (1996), Maleski and Martinez (2018), Skeeter et al. (2019), and Wang and Asefa (2018). And among all indices, this study finds Niño3.4 to be the strongest predictor in winter for PI and P90. This study finds weak correlations between the PNA and winter precipitation in the ACF, thereby showing that the ACF region is likely in a PNA-effects transition zone: strong negative correlations exist north and west of the ACF (Henderson and Vega 1996; Burt et al. 2018) and strong positive correlations exist southeast of the ACF (Henderson and Vega 1996).

5.2 The ACF basin has been getting wetter and is projected to get wetter

This study shows that the ACF basin has been getting wetter for the most part, with summer having the largest increases in PT and PD and thus large decreases in maximum CDD. While multiple studies note increasing precipitation annually (Michaels et al. 2004; Li et al. 2022) or during autumn (Powell and Keim 2015; Easterling et al. 2017; Bishop et al. 2019) for the SEUS in general, no other studies report increased summer precipitation. One reason for the uniqueness of this study's findings might be its time period of 1980–2021, which is a much more recent time period compared to others. Some studies do have a relatively recent ending year (Skeeter et al. 2019; Brown et al. 2019; Li et al. 2022); however, the starting years are either 1950 or 1960. This study also shows that heavy precipitation has generally increased, and that the significant increases tend to be confined to the northern portion of the basin. Previous studies (Wang et al. 2010; Skeeter et al. 2019; Bishop et al. 2019; Brown et al. 2019; Wang et al. 2021) also show an increase in heavy precipitation either annually or seasonally in the SEUS. The increased summer precipitation totals and frequencies and associated decrease in the length of dry periods should be positive news to various stakeholders in the basin, since increased summer precipitation can reduce the severity of soil-water deficits during June–September (Diem et al. 2021). Nevertheless, severe droughts have occurred recently (Williams et al. 2017), thereby illustrating that—especially with the increased water demand—it only takes a dry spring and summer to cause water shortages in the basin.

The precipitation projections for the ACF basin are similar to what other studies show for the SEUS. At the annual scale, there is agreement among all studies that PT and heavy-precipitation variables will increase (Almazroui et al. 2021; Douville et al. 2021; Marvel et al. 2021; Rastogi et al. 2022). The increased heavy precipitation is not surprising, since nearly all land areas globally should receive increased heavy precipitation (Douville et al. 2021). Further, this study agrees with the following additional findings in Douville et al. (2021): precipitation during all seasons will increase,

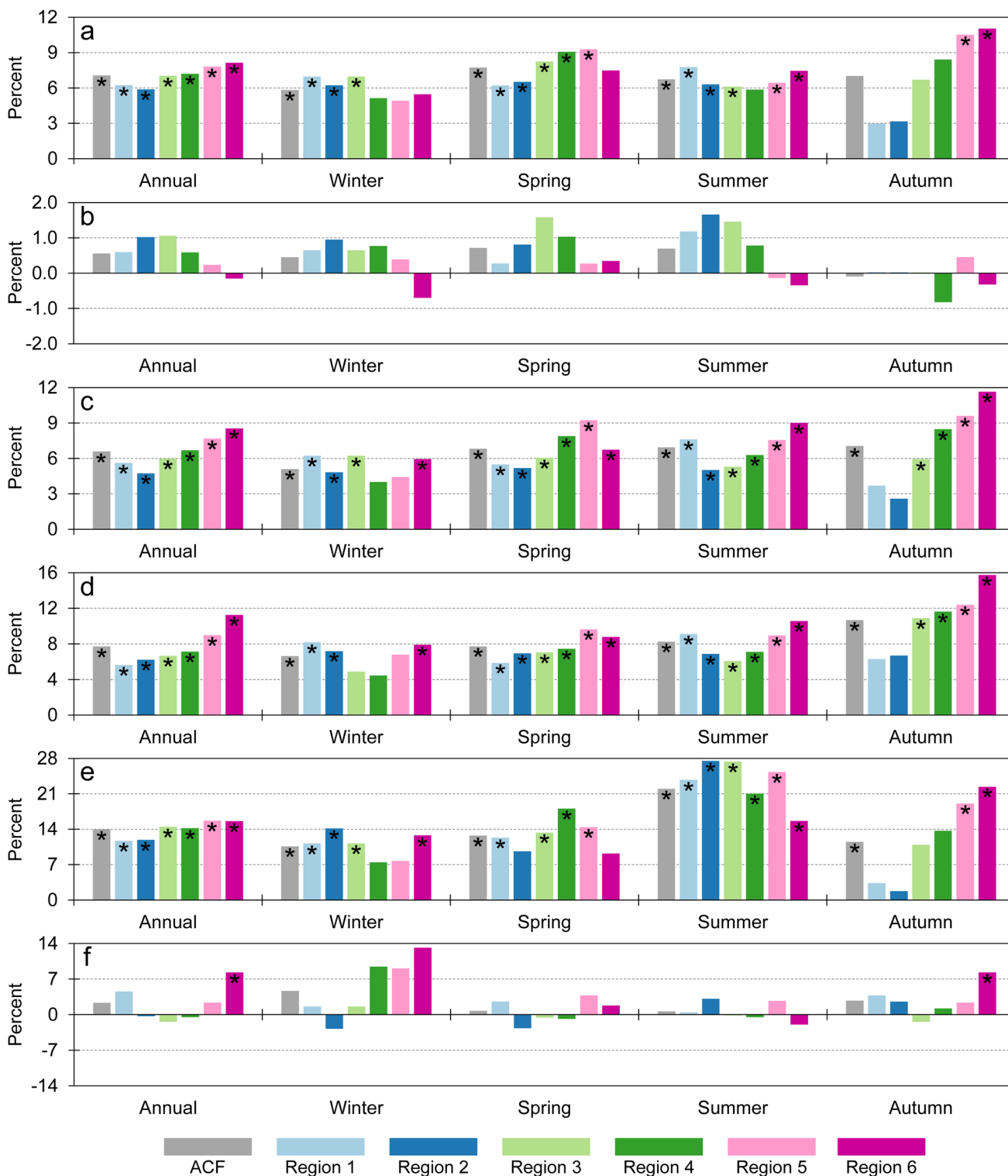


Fig. 8 Annual- and season-specific percent changes from 1980–2019 to 2020–2059 in **a** precipitation totals, **b** precipitation days, **c** precipitation intensity, **d** the 90th percentile of daily precipitation totals, **e** heavy-precipitation days, and **f** maximum consecutive dry days.

Asterisks denote significant ($\alpha = 0.05$; two tailed) differences in values between the two epochs. Full names of the precipitation variables are provided in the caption for Fig. 2

and the increase in precipitation intensity is much stronger than the increase in precipitation days. Increased precipitation intensity should not be welcomed by stakeholders in the basin, since—among other impacts—it will increase soil erosion (Eekhout and de Vente 2022) and the chance of floods (Blenkinsop et al. 2021).

5.3 There is general agreement between recent precipitation trends and model-derived projections

Recent precipitation trends and model-derived precipitation projections are in good agreement with respect to increasing PT and PD, moderate agreement with respect to increasing values of the heavy-precipitation variables, and poor agreement with respect to changes in maximum CDD (Figs. 5 and 8). Approximately 80% and 70% of combinations of spatial domain and temporal unit have the same current and projected directions of change for PT and PD, respectively. Recent changes in PT and PD are weaker and stronger, respectively, than projected changes in those variables. The agreement percentages decrease to between 50 and 60% for the heavy-precipitation variables. As should be expected, projected changes in heavy precipitation are much stronger and much more consistently positive compared to recent changes. Approximately 40% of the combinations have the same current and projected directions of change for maximum CDD. The projected changes in maximum CDD for spring and summer are weak and do not have consistent changes across the basin, while the current trends for maximum CDD in those two seasons are strong and show definite decreases and increases for spring and summer, respectively.

5.4 How will the Bermuda High change in the future?

Since indices of the Bermuda High are major drivers of precipitation variability in the ACF and are strongly correlated with precipitation throughout the SEUS, it is important to understand how the Bermuda High will change in the future. The western ridge is projected to be in a more westward position at the end of the century, which might cause more precipitation extremes in the SEUS (Li et al. 2011). The Bermuda High in general also is projected to shift westward (Li et al. 2012; Shaw and Voigt 2015; Cherchi et al. 2018). The consensus about future changes in the Bermuda High seems paradoxical, given that there is disagreement about its recent changes: Li et al. (2011) note that the western ridge moved significantly westward from the late 1970s to 2007, while Diem (2013a,b) reports a significant eastward shift over the same time period. This study confirms the findings in Diem et al. (2013b) by showing that during 1980–2021 the western ridge was moving eastward at a rate of $0.8^\circ \text{ decade}^{-1}$.

The eastward movement of the BHI has been hypothesized as the cause of increased summer precipitation days (Diem 2013a). Nevertheless, this study shows that the BHI and the WBHI, rather than the location of the western ridge, are the principal drivers of precipitation variability and might be causing the increased precipitation during summer. Therefore, it seems important to understand more fully how the BHI, WBHI, and—to a lesser degree—the location of the western ridge will change with increased global warming.

6 Conclusions

Through the analysis of precipitation variables at annual and seasonal scales for six regions in the ACF basin, this study has shown that the basin has been getting wetter and the trend is projected to continue for the next several decades to the end of the century. The analyses in this study cannot attribute the trends over the past several decades to global warming; rather, all that can be stated is that the trends have occurred within the most recent period of global warming. Precipitation totals and precipitation days tended to increase for all regions in the basin, but there were few significant trends. Increases in values of the heavy-precipitation variables were not as consistent as increases in precipitation totals and days; however, the northern portion of the basin—which likely has the most reliable results—did have multiple significant positive trends. All regions had increases and decreases in maximum consecutive dry days during spring and summer, respectively, with more significant trends existing for summer. Annual and seasonal values of the precipitation variables were typically strongly correlated with indices of the Bermuda High that showed the pressure gradient across the southwestern North Atlantic Ocean and southeastern United States, and those correlations were much stronger than the correlations with teleconnection indices. Therefore, linear regression analyses showed the strength and position of the Bermuda High to be the main driver of precipitation variability in the basin. Downscaled climate-model projections indicate that all regions in the basin should be wetter during the next several decades compared to the most recent several decades. Compared to recent changes in heavy-precipitation variables for the basin in general, projected changes in those variables are stronger and more consistently positive. The current trend of decreases in the maximum number of dry days in summer is not projected to continue. The projections should be treated with a fair amount of skepticism, since there is not strong agreement between the projections and current trends. Moreover, since the Bermuda High has had an outsized impact on precipitation in the basin and the southeastern United States in general, more information is needed about specific changes to the Bermuda High—and associated indices—in upcoming decades to better determine how precipitation might change.

Author contributions Both authors contributed to the study conception and design. Material preparation, data collection, and analysis were performed by J.D. and P.O.B. The first draft of the manuscript was written by J.D.

Data availability The data used in the study are available at <https://data.mendeley.com/datasets/d7b9dvjw4v/1>.

Declarations

Competing interests The authors declare no competing interests.

References

- Abatzoglou JT, Dobrowski SZ, Parks SA, Hegewisch KC (2018) TerraClimate, a high-resolution global dataset of monthly climate and climatic water balance from 1958–2015. *Sci Data* 5:170191. <https://doi.org/10.1038/sdata.2017.191>
- Allan RP, Willett KM, John VO, Trent T (2022) Global changes in water vapor 1979–2020. *J Geophys Res Atmos* 127:e2022JD036728. <https://doi.org/10.1029/2022JD036728>
- Almazroui M, Islam MN, Saeed F et al (2021) Projected changes in temperature and precipitation over the United States, Central America, and the Caribbean in CMIP6 GCMs. *Earth Syst Environ* 5:1–24. <https://doi.org/10.1007/s41748-021-00199-5>
- Atlanta Regional Commission (2020). Population and employment forecasts. <https://atlantaregional.org/atlanta-region/population-employment-forecasts/>
- Beck HE, Zimmermann NE, McVicar TR et al (2018) Present and future Köppen-Geiger climate classification maps at 1-km resolution. *Sci Data* 5:180214. <https://doi.org/10.1038/sdata.2018.214>
- Bishop DA, Williams AP, Seager R (2019) Increased fall precipitation in the southeastern United States driven by higher-intensity, frontal precipitation. *Geophys Res Lett* 46:8300–8309. <https://doi.org/10.1029/2019GL083177>
- Blenkinsop, S, Muniz Alves, L, Smith, AJP (2021). ScienceBrief Review: Climate change increases extreme rainfall and the chance of floods. In: C. C Le Quéré, P. P Liss, Forster P (eds) *Critical Issues in Climate Change Science*. <https://doi.org/10.5281/zenodo.4779119>
- Brown VM, Keim BD, Black AW (2019) Climatology and trends in hourly precipitation for the southeast United States. *J Hydrometeorol* 20:1737–1755. <https://doi.org/10.1175/JHM-D-19-0004.1>
- Burt TP, Ford Miniati C, Laseter SH, Swank WT (2018) Changing patterns of daily precipitation totals at the Coweeta Hydrologic Laboratory, North Carolina, USA. *Int J Climatol* 38:94–104. <https://doi.org/10.1002/joc.5163>
- Census Bureau US (1996) Population of the states and counties of the United States: 1790–1990. U.S. Census Bureau, Washington, D.C.
- Chattahoochee River Keeper (2023). The Lake Lanier equation. <https://chattahoochee.org/blog/the-lake-lanier-equation/>
- Cherchi A, Ambrizzi T, Behera S et al (2018) The response of subtropical highs to climate change. *Curr Clim Change Rep* 4:371–382. <https://doi.org/10.1007/s40641-018-0114-1>
- Davis SM, Rosenlof KH (2012) A multidagnostic intercomparison of tropical-width time series using reanalyses and satellite observations. *J Clim* 25:1061–1078. <https://doi.org/10.1175/JCLI-D-11-00127.1>
- Diem JE (2013a) Influences of the Bermuda High and atmospheric moistening on changes in summer rainfall in the Atlanta, Georgia region, USA. *Int J Climatol* 33:160–172. <https://doi.org/10.1002/joc.3421>
- Diem JE (2013b) Comments on “Changes to the North Atlantic Subtropical High and its role in the intensification of summer rainfall variability in the southeastern United States.”. *J Clim* 26:679–682. <https://doi.org/10.1175/JCLI-D-11-00390.1>
- Diem JE, Pangle LA, Milligan RA, Adams EA (2021) Intra-annual variability of urban effects on streamflow. *Hydrol Process* 35:35e14371. <https://doi.org/10.1002/hyp.14371>
- Douville H, Raghavan K, Renwick J et al (2021) Water cycle changes. In: Masson-Delmotte V, Zhai P, Pirani A, Connors SL, Péan C, Berger S, Caud N, Chen Y, Goldfarb L, Gomis MI, Huang M, Leitzell K, Lonnoy E, JBR M, Maycock TK, Waterfield T, Yelekçi O, Yu R, Zhou B (eds) *Climate change 2021: The physical science basis. Contribution of working group I to the sixth assessment report of the Intergovernmental Panel on Climate Change*. Cambridge University Press, Cambridge, United Kingdom and New York, NY, USA, pp 1055–1210. <https://doi.org/10.1017/9781009157896.010>
- Easterling DR, Arnold JR, Knutson T, et al (2017) Ch. 7: Precipitation change in the United States. *Climate Science Special Report: Fourth National Climate Assessment, Volume I*. U.S. Global Change Research Program. <https://science2017.globalchange.gov/chapter/7/>
- Easterling DR, Peterson TC (1995) A new method for detecting undocumented discontinuities in climatological time series. *Int J Climatol* 15:369–377. <https://doi.org/10.1002/joc.3370150403>
- Eekhout JPC, De Vente J (2022) Global impact of climate change on soil erosion and potential for adaptation through soil conservation. *Earth-Science Reviews* 226:103921. <https://doi.org/10.1016/j.earscirev.2022.103921>
- Feldman DL (2008) Barriers to adaptive management: Lessons from the Apalachicola-Chattahoochee-Flint Compact. *Soc & Nat Resour* 21:512–525. <https://doi.org/10.1080/08941920801905344>
- GISTEMP Team (2023) GISS Surface Temperature Analysis (GIS-TEMP), version 4. NASA Goddard Institute for Space Studies Dataset accessed 2023-07-31 at <https://data.giss.nasa.gov/gistemp/>
- Helsel DR, Hirsch RM (2002) *Statistical methods in water resources*. In: Hydrologic Analysis and Interpretation. U.S. Geological Survey, Washington, DC
- Henderson KG, Vega AJ (1996) Regional precipitation variability in the southern United States. *Phys Geogr* 17:93–112. <https://doi.org/10.1080/02723646.1996.10642576>
- Jamshidi Z, Samani N (2022) Mapping the spatiotemporal diversity of precipitation in Iran using multiple statistical methods. *Theor Appl Climatol* 150:893–907. <https://doi.org/10.1007/s00704-022-04191-5>
- Jiménez-de-la-Cuesta D, Mauritsen T (2019) Emergent constraints on Earth’s transient and equilibrium response to doubled CO₂ from post-1970s global warming. *Nat Geosci* 12:902–905. <https://doi.org/10.1038/s41561-019-0463-y>
- Kachigan SK (1991) *Multivariate statistical analysis: A conceptual introduction*. Radius, New York
- Kao SC, Ashfaq M, Rastogi D, Gangrade S (2022) CMIP6-based multi-model hydroclimate projection over the conterminous US. Hydro-Source. Oak Ridge National Laboratory, Oak Ridge, Tennessee, USA. <https://doi.org/10.21951/SWA9505V3/1887469>
- Kunkel KE, Stevens LE, Stevens SE, et al (2013). Regional climate trends and scenarios for the U.S. National Climate Assessment. Part 2. Climate of the Southeast U.S. NOAA Technical Report NESDIS 142-2.
- Lai H-W, Chen HW, Kukulies J et al (2021) Regionalization of seasonal precipitation over the Tibetan Plateau and associated large-scale atmospheric systems. *J Clim* 34:2635–2651. <https://doi.org/10.1175/JCLI-D-20-0521.1>
- Lawrence, SJ (2016). Water use in the Apalachicola-Chattahoochee-Flint River Basin, Alabama, Florida, and Georgia, 2010, and water-use

- trends, 1985–2010. Scientific investigations report 2016-5007. U.S. Geological Survey.
- Li M, Sun Q, Lovino MA et al (2022) Non-uniform changes in different daily precipitation events in the contiguous United States. *Weather and Climate Extremes* 35:100417. <https://doi.org/10.1016/j.wace.2022.100417>
- Li W, Li L, Fu R et al (2011) Changes to the North Atlantic Subtropical High and its role in the intensification of summer rainfall variability in the southeastern United States. *J Clim* 24:1499–1506. <https://doi.org/10.1175/2010JCLI3829.1>
- Li W, Li L, Ting M, Liu Y (2012) Intensification of Northern Hemisphere subtropical highs in a warming climate. *Nat Geosci* 5:830–834. <https://doi.org/10.1038/ngeo1590>
- Maleski JJ, Martinez CJ (2018) Coupled impacts of ENSO AMO and PDO on temperature and precipitation in the Alabama-Coosa-Tallahapoosa and Apalachicola-Chattahoochee-Flint river basins. *Int J Climatol* 38:e717–e728. <https://doi.org/10.1002/joc.5401>
- Marston ML, Ellis AW (2020) Delineating precipitation regions of the contiguous United States from cluster analyzed gridded data. *Ann Assoc Am Geogr* 111(6):1721–1739. <https://doi.org/10.1080/24694452.2020.1828803>
- Marvel K, Cook BI, Bonfils C et al (2021) Projected changes to hydroclimate seasonality in the continental United States. *Earth's Future* 9:e2021EF002019. <https://doi.org/10.1029/2021EF002019>
- Michaels PJ, Knappenberger PC, Frauenfeld OW, Davis RE (2004) Trends in precipitation on the wettest days of the year across the contiguous USA. *Int J Climatol* 24:1873–1882. <https://doi.org/10.1002/joc.1102>
- Mitra S, Srivastava P, Singh S (2016) Effect of irrigation pumpage during drought on karst aquifer systems in highly agricultural watersheds: example of the Apalachicola-Chattahoochee-Flint river basin, southeastern USA. *Hydrogeol J* 24:1565–1582. <https://doi.org/10.1007/s10040-016-1414-y>
- Nigam S, Guan B, Ruiz-Barradas A (2011) Key role of the Atlantic Multi-decadal Oscillation in 20th century drought and wet periods over the Great Plains. *Geophys Res Lett* 38:L16713. <https://doi.org/10.1029/2011GL048650>
- O’Gorman PA, Schneider T (2009) The physical basis for increases in precipitation extremes in simulations of 21st-century climate change. *Proc Natl Acad Sci USA* 106:14773–14777. <https://doi.org/10.1073/pnas.0907610106>
- Powell EJ, Keim BD (2015) Trends in daily temperature and precipitation extremes for the southeastern United States: 1948–2012. *J Clim* 28:1592–1612. <https://doi.org/10.1175/JCLI-D-14-00410.1>
- Rastogi D, Kao S, Ashfaq M (2022) How may the choice of downscaling techniques and meteorological reference observations affect future hydroclimate projections? *Earth's Future* 10:e2022EF002734. <https://doi.org/10.1029/2022EF002734>
- Schlef KE, Steinschneider S, Brown CM (2018) Spatiotemporal impacts of climate and demand on water supply in the Apalachicola-Chattahoochee-Flint Basin. *J Water Resour Plann Manage* 144:05017020. [https://doi.org/10.1061/\(ASCE\)WR.1943-5452.0000865](https://doi.org/10.1061/(ASCE)WR.1943-5452.0000865)
- Schmitz F, McCreary T (2022) To court without the Corps? The U.S. Army Corps of Engineers and Florida v. Georgia. *Southeast Geogr* 62:298–317. <https://doi.org/10.1353/sgo.2022.0035>
- Seager R, Tzanova A, Nakamura J (2009) Drought in the southeastern United States: Causes, variability over the last millennium, and the potential for future hydroclimate change. *J Clim* 22:5021–5045. <https://doi.org/10.1175/2009JCLI2683.1>
- Skeeter WJ, Senkbeil JC, Keellings DJ (2019) Spatial and temporal changes in the frequency and magnitude of intense precipitation events in the southeastern United States. *Int J Climatol* 39:768–782. <https://doi.org/10.1002/joc.5841>
- Stahle DW, Cleaveland MK (1992) Reconstruction and analysis of spring rainfall over the Southeastern U.S. for the past 1000 years. *Bull Amer Meteor Soc* 73:1947–1961. [https://doi.org/10.1175/1520-0477\(1992\)073<1947:RAAOSR>2.0.CO;2](https://doi.org/10.1175/1520-0477(1992)073<1947:RAAOSR>2.0.CO;2)
- Thornton MM, Shrestha R, Wei Y et al (2022) Daymet: Daily surface weather data on a 1-km grid for North America, version 4 R1. ORNL DAAC, Oak Ridge, Tennessee, USA. <https://doi.org/10.3334/ORNLDAAC/2129>
- Trenberth K (2011) Changes in precipitation with climate change. *Clim Res* 47:123–138. <https://doi.org/10.3354/cr00953>
- Trenberth KE (1997) The definition of El Niño. *Bull Amer Meteor Soc* 78:2771–2777. [https://doi.org/10.1175/1520-0477\(1997\)078<2771:TDOENO>2.0.CO;2](https://doi.org/10.1175/1520-0477(1997)078<2771:TDOENO>2.0.CO;2)
- Trewartha GT, Horn LH (1980) An introduction to climate. McGraw-Hill
- Wang H, Asefa T (2018) Impact of different types of ENSO conditions on seasonal precipitation and streamflow in the Southeastern United States. *Int J Climatol* 38:1438–1451. <https://doi.org/10.1002/joc.5257>
- Wang H, Asefa T, Erkyihun S (2021) Interannual variabilities of the summer and winter extreme daily precipitation in the Southeastern United States. *J Hydrol* 603:127013. <https://doi.org/10.1016/j.jhydrol.2021.127013>
- Wang H, Fu R, Kumar A, Li W (2010) Intensification of summer rainfall variability in the southeastern United States during recent decades. *J Hydrometeorol* 11:1007–1018. <https://doi.org/10.1175/2010JHM1229.1>
- Wetherald RT (2009) Changes of variability in response to increasing greenhouse gases. Part II: Hydrology. *J Clim* 22:6089–6103. <https://doi.org/10.1175/2009JCLI2834.1>
- Williams AP, Cook BI, Smerdon JE et al (2017) The 2016 Southeastern U.S. drought: An extreme departure from centennial wetting and cooling. *J Geophys Res Atmos* 122:10888–10905. <https://doi.org/10.1002/2017JD027523>
- Zhang Y, Moges S, Block P (2016) Optimal cluster analysis for objective regionalization of seasonal precipitation in regions of high spatial-temporal variability: Application to western Ethiopia. *J Clim* 29:3697–3717. <https://doi.org/10.1175/JCLI-D-15-0582.1>

Publisher's Note Springer Nature remains neutral with regard to jurisdictional claims in published maps and institutional affiliations.

Springer Nature or its licensor (e.g. a society or other partner) holds exclusive rights to this article under a publishing agreement with the author(s) or other rightsholder(s); author self-archiving of the accepted manuscript version of this article is solely governed by the terms of such publishing agreement and applicable law.